Research Article | Vol. 27, No. 16 | 5 Aug 2019 | OPTICS EXPRESS 23262
Optics EXPRESS

# Phase noise of frequency doublers in optical clock lasers

SOFIA HERBERS, SÖREN DÖRSCHER, ERIK BENKLER, AND CHRISTIAN LISDAT*

*Physikalisch-Technische Bundesanstalt, Bundesallee 100, 38116 Braunschweig, Germany*
**christian.lisdat@ptb.de*

**Abstract:** Frequency doublers are widely used in high-resolution spectroscopy to shift the operation wavelength of a laser to a more easily accessible or otherwise preferable spectral region. We investigate the use of a periodically-poled lithium niobate (PPLN) waveguide frequency doubler in an optical clock. We focus on the phase evolution between the fundamental (1396 nm) and frequency-doubled (698 nm) light and its effect on clock performance. We find that the excess phase noise of the doubler under steady-state operation is at least two orders of magnitude lower than the noise of today's best interrogation lasers. Phase chirps related to changes of the optical power in the doubler unit and their influence on the accuracy of optical clocks are evaluated. We also observe substantial additional noise when characterizing the doubler unit with an optical frequency comb instead of using two identical waveguide doublers.



## 1. Introduction

State-of-the-art optical clocks reach instabilities below $10^{-16}/\sqrt{\tau/\mathrm{s}}$ as well as fractional systematic uncertainties of about $10^{-18}$ [1–7]. Transportable optical clocks have gained in importance as they offer flexible measurement locations and thus allow applications in new fields such as chronometric leveling for relativistic geodesy [8, 9]. The instability of the best optical clocks is typically limited either by the clock laser frequency noise due to the Dick effect [10, 11] or by quantum projection noise [12], which both are linked to laser noise and coherence properties. Clock lasers are usually based on lasers pre-stabilized to ultrastable reference cavities. The stability of these cavities is fundamentally limited by thermal noise of their mirror coatings [13]. To push this limit, cavities are operated at cryogenic temperatures [14], extended in length [15, 16], or fitted with crystalline mirror coatings [17]. State-of-the-art ultra-stable silicon cavities reach a fractional frequency instability of $4 \times 10^{-17}$ [14]. These silicon cavities have to be operated in the spectral region of 1.5 µm. The same holds for crystalline mirror coatings which are currently only available in the infrared (IR) spectral region, as GaAs/AlGaAs-based crystalline mirror coatings are highly absorbing for visible light. The frequency stability of an ultrastable laser based on silicon cavities or on these mirrors must thus be transferred to the spectral region of interest either via an optical frequency comb [18, 19] or directly by harmonic generation. Here, the effect of the transfer process on the laser's phase must be considered carefully. Excess noise may degrade the clock laser stability or compromise the clock accuracy via phase chirps caused by intensity modulation.

We investigate the conversion of 1396 nm radiation to the clock transition frequency of strontium (Sr) at 698 nm by a compact and robust second-harmonic generation (SHG) module. This subharmonic wavelength allows the use of a reference cavity with crystalline mirrors, and thus superior frequency stability at a given length of the cavity. It is part of a transportable clock laser system based on a 20 cm-long cavity with a thermal noise floor of $1 \times 10^{-16}$ for PTB's transportable optical clock [20]. The SHG module is a commercial fiber-to-free-space doubler (NTT Electronics) based on a PPLN waveguide.

Several physical effects can cause excess noise of a SHG module. Amplitude-to-phase

#367797 https://doi.org/10.1364/OE.27.023262
Journal © 2019 Received 23 May 2019; revised 9 Jul 2019; accepted 13 Jul 2019; published 30 Jul 2019

Optics EXPRESS

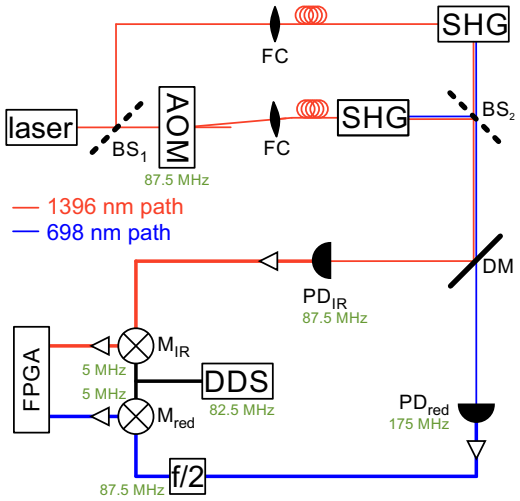


Fig. 1. Schematic sketch of the experimental setup used to determine the excess phase noise of two second-harmonic generator (SHG) modules. BS: beam splitter, DM: dichroic mirror, PD: photodiode, AOM: acousto-optical modulator, $f/2$ frequency divider, DDS: direct digital synthesizer, M: frequency mixer, FPGA: field-programmable gate array. FC: fiber coupler.

conversion originates from changes of the differential refractive index of the SHG material due to the induced temperature fluctuations. They can also be caused by the Kerr effect, i.e., intensity-dependent phase shifts, based either on the material's inherent nonlinear susceptibility $\chi^{(3)}$ or that resulting from cascaded $\chi^{(2)}$ processes [21]. A more fundamental limit is caused by thermal noise as described in [22].

Within this paper, we characterize excess phase noise and chirps introduced by the SHG module by comparing the outputs of two identical modules and discuss our results (section 2). In section 3, we present the results of a similar measurement using frequency transfer via an optical femtosecond frequency comb. The implications of our findings on clock performance when using a simple setup for a path length stabilization are discussed in section 4.

## 2. Phase noise measurement using two SHG modules

### 2.1. Experimental setup

Excess phase noise between fundamental and doubled light is analyzed by beating the fundamental and second harmonic waves of two SHG modules with each other as shown in Fig. 1. Besides laser noise and noise from the acousto-optical modulator (AOM), excess noise can result from uncompensated optical path length fluctuations. Our setup enables us to strongly suppress these contributions by using the fundamental light (1396 nm) transmitted through the doublers along with the second harmonic light (698 nm): fundamental light from the cw laser with frequency

$$\nu_L(t) = \nu_0 + \Delta\nu(t), \tag{1}$$

where $\nu_0$ is the mean laser frequency and $\Delta\nu(t)$ is its frequency noise, is split at beam splitter 1 ($BS_1$) and fed to two fiber-coupled SHG-modules. One path is frequency-shifted and power-controlled by an AOM with a radio frequency (rf) of $f_0$ and frequency noise $\Delta f(t)$. Therefore, the fundamental light entering the second SHG module has the frequency

$$\nu'_L(t) = \nu_0 + \Delta\nu(t) + f_0 + \Delta f(t). \tag{2}$$

The fundamental and second-harmonic beams overlap at the SHG modules' outputs. The beams from both SHG modules are superimposed on the beam splitter $BS_2$. The two wavelengths are then separated using a dichroic mirror (DM). The beat frequency $f_{IR}$ at photodiode (PD) $PD_{IR}$ between the fundamental beams is given by the AOM's frequency and noise.

$$f_{IR} = \nu'_L - \nu_L = f_0 + \Delta f(t) \tag{3}$$

Likewise, the beat frequency $f_{red}$ at $PD_{red}$ is

$$f_{red} = 2(\nu'_L + \Delta\nu_{SHG,\,1}) - 2(\nu_L + \Delta\nu_{SHG,\,2}) = 2f_0 + 2\Delta f + 2\Delta\nu_{SHG,\,1} - 2\Delta\nu_{SHG,\,2}, \tag{4}$$

where $\Delta\nu_{SHG,\,1}$ and $\Delta\nu_{SHG,\,2}$ denote the noise caused by the cw SHG modules. While the laser noise $\Delta\nu$ cancels out for both beat signals, $\Delta f$, $\Delta\nu_{SHG,\,1}$ and $\Delta\nu_{SHG,\,2}$ remain. The detected beat frequency $f_{red}$ is divided by two. Both beat signals are mixed down to 5 MHz using a DDS referenced to a hydrogen maser. An FPGA digitizes the 5 MHz inputs with a sample rate of 100 MHz and records the differential phase evolution of the input signals, from which we calculate the combined phase noise power spectral density (PSD). The noise contribution $\Delta f$ cancels out, while $\Delta\nu_{SHG,\,1}$ and $\Delta\nu_{SHG,\,2}$ persist and lead to the differential frequency noise

$$\Delta\nu_{exc} = \Delta\nu_{SHG,\,1} - \Delta\nu_{SHG,\,2}. \tag{5}$$

Phase noise caused by path length fluctuations is subdivided in three parts of the setup: The noise caused by path length fluctuations between $BS_1$ and the SHG modules enters in the same way as $\Delta f$ and thus cancels out. Secondly, between the SHG modules and DM, the red and IR beams propagate in common path. Therefore, path length fluctuations affect the two wavelengths in an equivalent fashion except for negligible dispersion effects and cancel, too. Thirdly, between DM and PDs, the red and IR beams, respectively, propagate on a common path. Hence, the path length fluctuations are equal in each pair of beams and thus cancel in the beat signals on the PDs. Note that differential delays between separated path segments causes noise suppression to break down for frequencies similar to or above the inverse time delay. In addition, some noise, e.g. caused by ambient temperature fluctuations, is common-mode and thus rejected in this setup, while it can be an issue for the optical clock setup, which is discussed in section 4.

In short, the setup shown in Fig. 1 allows us to measure the phase noise between fundamental and frequency-doubled light of our SHG modules while laser noise, AOM noise, and noise caused by path length fluctuations are rejected.

### 2.2. Phase noise measurement

We first characterize the electronic noise of the experimental setup by replacing the PDs by two synthesizers, which are referenced to a hydrogen maser and set to the same frequencies and output power levels as the beat signals detected by the PDs. The result is shown in Fig. 2 (green line). Additional detection noise from photon shot noise is expected to result in a white phase noise floor at about $5 \cdot 10^{-11}$ rad$^2$/Hz.

The PSD of the measured excess frequency noise $\Delta\nu_{exc}$ is shown in Fig. 2 (blue curve) along with the PSD of the laser locked to PTB's silicon cavity (red line) [14], which is one of the most stable lasers today. $\Delta\nu_{exc}$ is considerably below the laser noise. Thus, the frequency conversion does not degrade the laser performance. Frequencies below 10 Hz are particularly relevant for optical clock operation because of their influence on the clock instability due to the Dick effect [6, 11]. The PSD of the excess noise $\Delta\nu_{exc}$ is $4 \cdot 10^{-5}$ rad$^2$/Hz at a frequency of 0.1 Hz and decreases to $1 \cdot 10^{-9}$ rad$^2$/Hz at a few Hz, where it reaches the electrical noise floor. For frequencies of a few hundreds of hertz, additional noise matching the expected photon shot noise floor is observed.

Optics EXPRESS

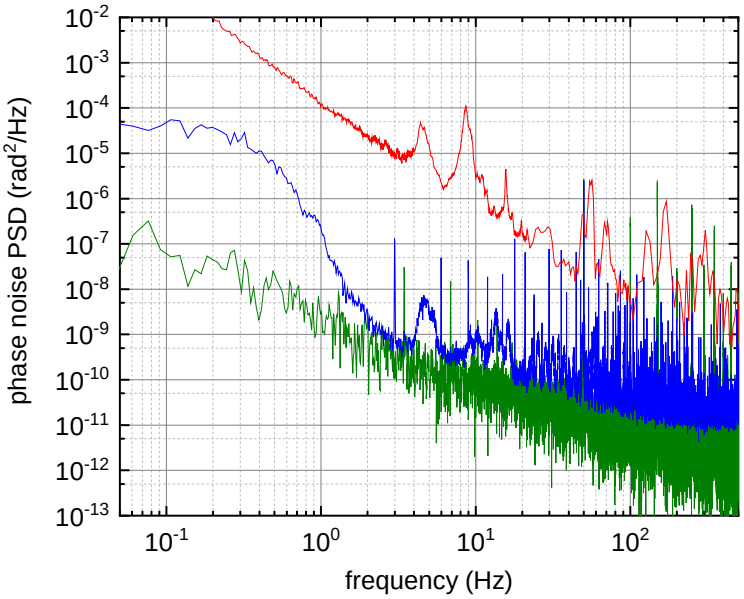


Fig. 2. Power spectral density (PSD) of the electronic noise of the experimental setup (green line), PSD of phase noise between fundamental and doubled light of SHG modules $\Delta\nu_{\mathrm{exc}}$ (blue line), and PSD of laser noise of a laser stabilized to PTB's silicon cavity (red line) [14]

Our results yield a limit on doubler-induced phase noise that is lower than a comparable characterization by Delehaye et al. [23] by at least 13 dB for frequencies smaller than 1 Hz and by two to four orders of magnitude for frequencies between 1 Hz and 10 Hz. Delehaye et al. investigate the phase noise of a SHG module at 871 nm, also manufactured by NTT Electronics. The authors of that study suggest differential path length fluctuations related to the use of an acousto-optic modulator (AOM) as an additional source of noise. There, the AOM was placed behind the SHG module rather than in front of the SHG module as in our setup. The noise power spectral density observed in [23] would indeed pose a limitation for state-of-the-art lasers such as [14].

Yeaton-Massey et al. [22] investigates the relative frequency fluctuations in SHG of a periodically poled potassium titanyl phosphate (PPKTP) crystal at 1064 nm. Our resulting phase noise PSD is approximately one order of magnitude below the phase noise PSD at 1064 nm calculated from the frequency noise given in [22] for frequencies between 0.1 Hz and 10 Hz. As different SHG devices are used, a comparison is reasonable only to a limited extent.

Our measurement shows that the phase noise PSD of the SHG module is at least two orders of magnitude lower than today's best clock lasers [14] for frequencies lower than 10 Hz.

## 3. Phase noise measurement using a frequency comb

### 3.1. Experimental setup

Frequency combs can be used for stability transfer where SHG is not feasible. They also offer greater overall flexibility in the choice of spectral region, especially in case of stability transfer from a single master laser to multiple laser frequencies.

Optics EXPRESS

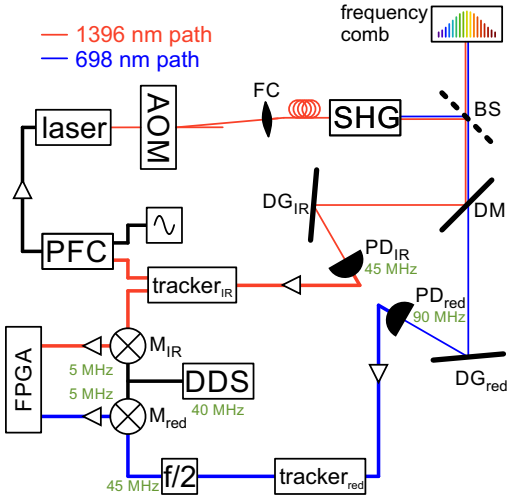


Fig. 3. Schematic sketch of the experimental setup to determine the excess phase noise of a second-harmonic generation (SHG) module and a frequency comb. BS: beam splitter, DM: dichroic mirror, DG: diffraction grating, PD: photo diode, tracker: narrow-band filter (band width 500 kHz) and amplifier consisting of a phase-locked loop using a voltage-controlled oscillator that follows the input frequency, PFC: phase frequency comparator, AOM: acousto-optical modulator, $f/2$ frequency divider, DDS: direct digital synthesizer, M: frequency mixer, FPGA: field-programmable gate array, FC: fiber coupler.

Therefore, we investigate the phase noise between fundamental and frequency-doubled light as shown in Fig. 3, by beating the SHG module's output with the light from a frequency comb in a transfer oscillator setup [24]. Within this scheme, the comb itself is not optically locked and its modes have individual line widths of up to 100 kHz. In contrast to the previous section, tracking oscillators, which follow the frequency and phase within the bandwidth of their phase-locked loop, are required because the beat notes now have lower signal-to-noise ratio. This is due to the limited comb line power and particularly due to spatial mode mismatches between the output of the SHG module and comb's output (see below). The cw laser is locked to the comb with a low bandwidth so as to keep all beat notes in their respective detection windows. The frequency of the n$^{\text{th}}$ comb line is described by

$$\nu_{\mathrm{n}} = \nu_{\mathrm{CEO}} + \Delta\nu_{\mathrm{CEO}} + n(f_{\mathrm{rep}} + \Delta f_{\mathrm{rep}}), \tag{6}$$

with $|\nu_{\mathrm{CEO}}| < f_{\mathrm{rep}}$, where $\nu_{\mathrm{CEO}}$ is the carrier-envelope offset (CEO) frequency and $\Delta\nu_{\mathrm{CEO}}$ its noise, $n$ is an integer, $f_{\mathrm{rep}}$ is the pulse repetition rate, and $\Delta f_{\mathrm{rep}}$ its noise. The fundamental comb around 1560 nm is broadened in a highly nonlinear fiber to 1396 nm and beyond, from which a comb spectrum around 698 nm and with a width of approximately 3 nm is generated using a free-space-coupled PPLN crystal. A comb line near 698 nm is generated by sum frequency generation (SFG) from all suitable comb line pairs within the phase matching bandwidth of the PPLN crystal. The spectrum of the visible light $\nu_m$ is described by

$$\nu_{\mathrm{m}} = 2 \times (\nu_{\mathrm{CEO}} + \Delta\nu_{\mathrm{CEO}}) + m(f_{\mathrm{rep}} + \Delta f_{\mathrm{rep}}) + \Delta\nu_{\mathrm{SFG,\,m}}. \tag{7}$$

Similarly to the discussion in section 2, comb noise, laser noise, AOM noise and noise caused by path length fluctuations cancel out. Only the doubler noise $\Delta\nu_{\mathrm{SHG,\,1}}$ and noise caused by generating the visible light from the IR comb spectrum, $\Delta\nu_{\mathrm{SFG,\,m}}$, persist in the differential phase

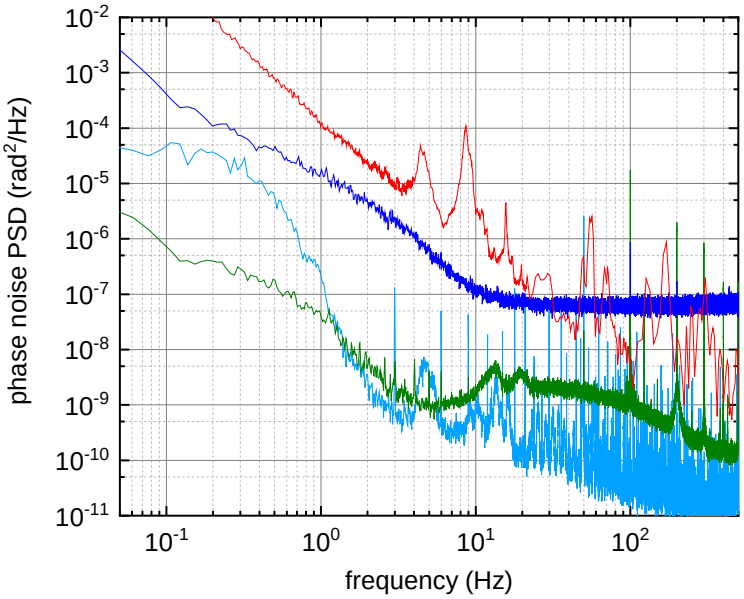


Fig. 4. Power spectral density (PSD) of the electronic noise of the experimental setup (green line), PSD of phase noise from the comb measurement (blue line) and the SHG module measurement in section 2 (light blue line), PSD of laser noise of a laser stabilized to PTB's silicon cavity (red line) [14]

evolution. Thus, the excess noise

$$\Delta\nu_{\mathrm{exc,\,2}} = \Delta\nu_{\mathrm{SHG,\,1}} - \Delta\nu_{\mathrm{SFG,\,m}} \tag{8}$$

is similar to Eq. (5).

### 3.2. Phase noise measurement

We use the setup shown in Fig. 3 to characterize the intrinsic electrical noise of the experimental setup as well as the phase noise between fundamental and frequency-doubled light, as in section 2. We expect a white phase noise floor at about $10^{-7}$ rad$^2$/Hz caused by photon shot noise.

The electronic noise of the experimental setup is shown in Fig. 4 (green line). The measured PSD of $\Delta\nu_{\mathrm{exc,\,2}}$ is shown as a blue line, along with the noise level of the silicon-cavity locked laser (red line) for comparison. The PSD of the excess noise $\Delta\nu_{\mathrm{exc,\,2}}$ is a few $10^{-4}$ rad$^2$/Hz at a frequency of 0.1 Hz and reaches a white phase noise floor of $10^{-7}$ rad$^2$/Hz at a Fourier frequency of 10 Hz, which is negligible for clock operation. The noise floor matches the expected level caused by photon shot noise.

The observed phase noise $\Delta\nu_{\mathrm{exc,\,2}}$ between fundamental light and doubled light in steady-state operation does not limit the clock laser stability for today's best clock lasers but is significantly higher than the PSD observed in our comparison of two SHG modules (light blue line in Fig. 4) as well as significantly higher than the PSD of a stability transfer measurement with an optical comb in [18], which is only comparable to a certain extent as the measurement in [18] does not include tracking oscillators or sum frequency generation. We conclude that the additional noise in the measurement is caused by the comb or the electronic signal processing. At Fourier

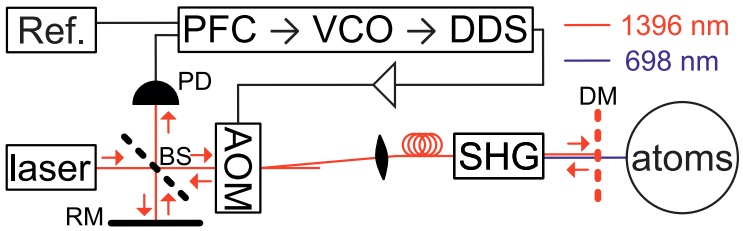


Fig. 5. Sketch of a simple path length stabilization including a second harmonic generation (SHG) module. RM: reference mirror BS: beam splitter, AOM: acousto-optical modulator, DM: dichroic mirror, PD: photo diode, Ref.: 100 MHz reference signal PFC: phase frequency comparator, VCO: voltage-controlled oscillator, DDS: direct digital synthesizer.

frequencies of a few Hz, the excess noise $\Delta\nu_{\mathrm{exc,\,2}}$ is only an order of magnitude below the noise of the Si-cavity stabilized laser. With the next generation of ultra-stable cavities outlined in [14], the limitation of stability transfer by a comb in this spectral region will become highly relevant for clock operation. The higher phase noise PSD of this measurement could result from amplitude to phase noise conversion in the sum frequency generation in the comb, by imperfect suppression of the comb's frequency noise in the transfer scheme, or by imperfect phase following of the tracking oscillators. Another reason could be residual differential path length fluctuations, as the IR light exiting the SHG modules is not collimated. Therefore, the overlap with the comb light is poor and the common path propagation is degraded. The overlap of IR light between two SHG modules may be better as both beams have similar divergences. The poor mode overlap does give rise to the increased photon shot noise floor in the comb measurement compared to the cw comparison in section 2.

## 4. Light pulse generation with frequency doublers

For practical reasons, optical fibers are used to transfer light from a clock laser to the atomic reference of an optical clock. Optical path length stabilization is indispensable to achieve fractional frequency instability below $1 \times 10^{-16}$ [25]. A simple path length stabilization as shown in Fig. 5 is of particular interest using PPLN frequency-doublers in transportable systems. Here, fundamental light reflected from a DM, for example the lattice retroreflection mirror in a lattice clock, is used for path length stabilization. Laser pulses for interrogation are generated by modulating the power of the fundamental wave in this scheme. Therefore, phase shifts between the fundamental and the frequency-doubled light, in particular in response to strong intensity modulations, cannot be compensated by this path length stabilization. These are critical as they result in a systematic frequency shifts of the clock.

We investigate the SHG module's response to step-like power changes using the same setup as in section 2 (see Fig. 1) and estimate the related error for typical operation conditions of optical clocks. Investigating these errors is important since, in contrast to the first sections of the paper, the effects discussed here not only add noise that can be compensated by additional averaging time but may introduce systematic offsets that falsify the measurement results. We change the input power of the SHG module by steps $\Delta P_{\mathrm{IR}}$ between 1 mW and 6 mW every 50 s using the AOM shown in Fig. 1. Stepping the input power results in a differential step in the absolute phase between fundamental and frequency-doubled light and transient oscillations of about 1 ms shortly after the power steps. The step in absolute phase results from power to phase conversion in our measurement electronics (in particular mixers and the frequency divider). The transient oscillations result from the frequency divider. Therefore, both are electronic artifacts and can be neglected if the relevant elements are not present in the actual path length stabilization setup.

To assess possible effects on clock operation, we consider potential settling of the phase

Optics EXPRESS

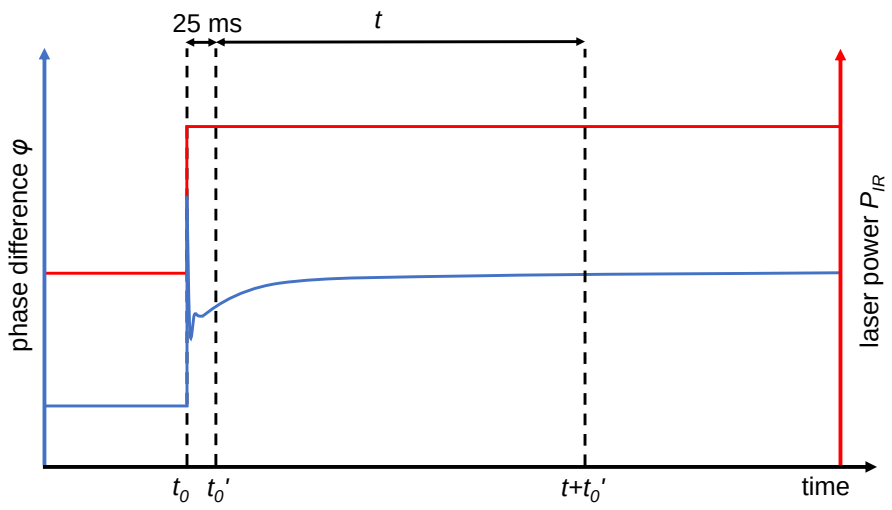


Fig. 6. Schematic sketch of the phase difference between fundamental and frequency-doubled light (blue line) in response to a input power step (red line).

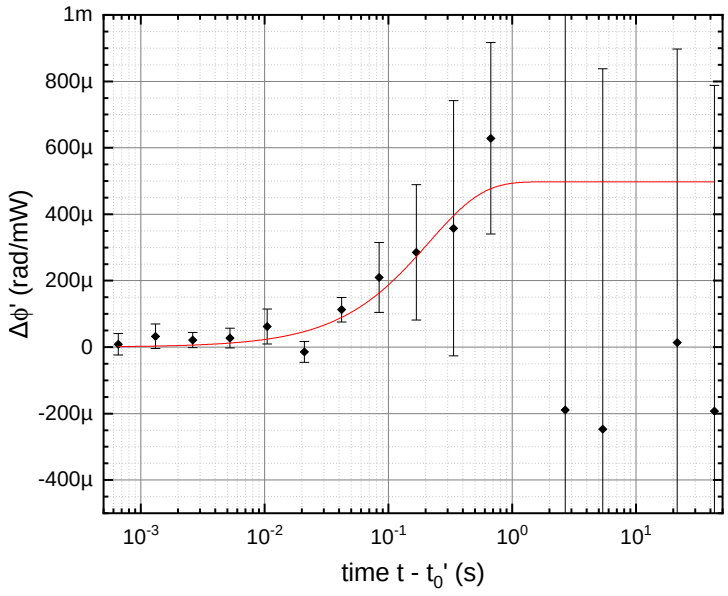


Fig. 7. Phase difference per 1 mW of laser power over a duration $t - t_0'$ after a power switching event, starting 25 ms after the power step. Black diamonds represent measured data averaged over ten samples. A model with exponential settling of the phase has been fitted to the data (red line).

Optics EXPRESS

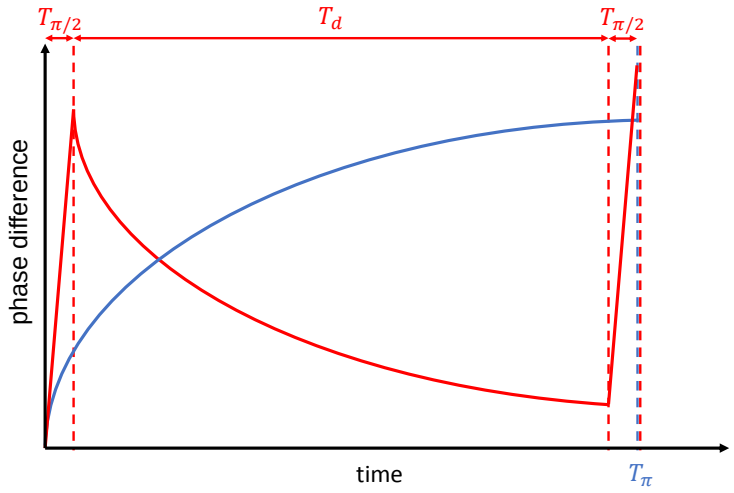


Fig. 8. Schematic phase difference between fundamental and frequency-doubled light for a Rabi (blue line) and Ramsey (red line) scheme.

difference over an extended period of time. Such an effect can originate from a variation of absorbed optical power and thus crystal temperature via the dependence of the refractive index on the temperature. In the simplest case, a step in optical power load $\Delta P_{\mathrm{IR}}$ at $t = 0$ causes a phase response normalized to $\Delta P_{\mathrm{IR}}$ of

$$\Delta\phi_{\mathrm{settle}}(t) = A(1 - e^{-t/\tau}). \tag{9}$$

We evaluate the phase response using a series of measurements with power steps of different magnitude. For each event, we compute the phase differences $\Delta\phi'(t, t_0') = [\varphi(t + t_0') - \varphi(t_0')]/\Delta P_{\mathrm{IR}}$ for various durations $t$ (see Fig. 6). We choose a reference time $t_0' = t_0 + 25$ ms after the power step (at $t_0$) for our analysis to exclude the fast transient. Fig. 7 shows the mean values of $\Delta\phi'(t, t_0')$ (black diamonds) and their uncertainties. Following Eq. (9), we fit $\Delta\phi'(t) = A'(1 - e^{-(t-t_0')/\tau})$ to the data (red line). We find $A = 56(28)\times 10^{-5}$ rad/mW and $\tau = 0.21(14)$ s, where $A = A' e^{(t_0'-t_0)/\tau}$.

We expect to find different influence on Rabi and Ramsey spectroscopy owing to the differences in typical pulse duration, pulse powers and sensitivities to phase chirps. Rabi spectroscopy consists of a single $\pi$-pulse of the duration $T_\pi$ with up to a few seconds length which requires low laser power. In contrast, Ramsey spectroscopy consists of two $\pi/2$-pulses of duration $T_{\pi/2}$ separated by the dark time of duration $T_d$. While the latter can be several seconds long, the excitation pulses are typically short ($T_{\pi/2} \approx 1$ ms). Therefore, high laser power is required. For more details, see [10, 26] among others. The phase evolution expected during Rabi spectroscopy and Ramsey spectroscopy, respectively, are schematically shown in Fig. 8. Note that, in the case of Ramsey spectroscopy, the phase returns to its zero-power value following Eq. (9) with the same time constant $\tau$ during the dark time and thus starts from a non-zero value during the second pulse.

To illustrate the phase amplitude for realistic operating conditions of an optical clock, we estimate the required power at the fundamental wavelength for the E1 transition in a strontium lattice clock: The laser power at 698 nm required for a $\pi$-pulse of duration $T_\pi$ is given by [27]

$$P_{\mathrm{red}} = \frac{\pi^4 h \nu^3 w_0^2}{3 A_{\mathrm{ki}} c^2} \times T_\pi^{-2} \tag{10}$$

Optics EXPRESS

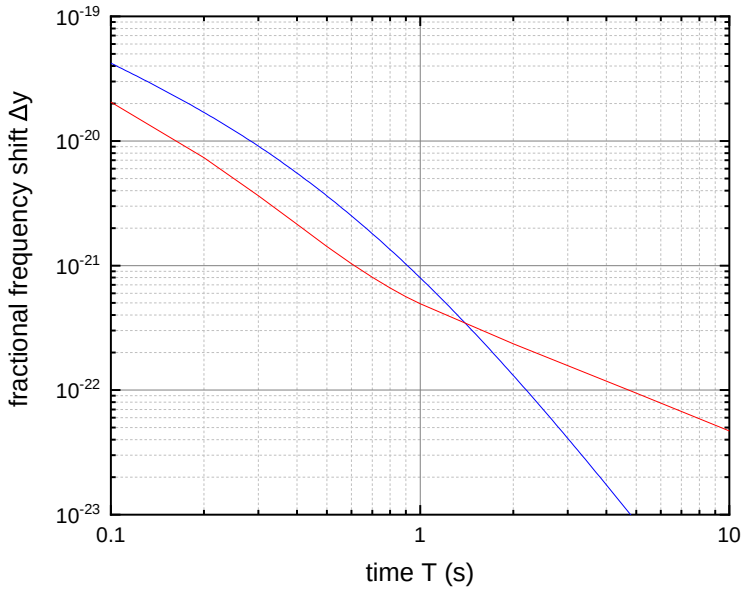


Fig. 9. Fractional frequency shift $\Delta y$ caused by phase evolution during Rabi interrogation with a duration $T_\pi = T$ (blue line) and for Ramsey interrogation with dark time $T_d = T$ and $T_{\pi/2} = 1$ ms, for a conversion efficiency $\eta = 3.8$ W$^{-1}$ and a waist radius $w_0 = 100$ µm. Note that $\Delta y$ is approximately proportional to $w_0$.

if we assume that the waist radius $w_0$ of the beam is much larger than the extent of the atomic sample. For our analysis, we use a realistic value of $w_0 = 100$ µm. In Eq. (10), $\nu \approx 429$ THz is the transition frequency, $A_{\mathrm{ki}} = 69(19) \times 10^{-4}$ s$^{-1}$ [28] the Einstein A coefficient of the $^1\mathrm{S}_0 \rightarrow {}^3\mathrm{P}_0$ transition in strontium, $h$ the Planck constant, and $c$ the speed of light in vacuum. We derive the required fundamental power using $P_{\mathrm{red}} = \eta P_{\mathrm{IR}}^2$ with doubling efficiency $\eta$. We use a doubling efficiency $\eta = 3.8$ W$^{-1}$, which is typical for this SHG module. Note, however, that we have observed variations between 1 W$^{-1}$ and 7 W$^{-1}$ in doubling efficiency for different modules.

To evaluate the clock errors due to the phase response we have to take into account the phase sensitivity of the different spectroscopy types. Thus we numerically integrated the Schrödinger equation to calculate the change of excitation probability $\Delta p$ caused by the phase evolution shown in Fig. 7. For a Rabi pulse of length $T_\pi$ at half a line width detuning, the resulting fractional frequency shift $\Delta y = \Delta p/(\pi\ \nu\ T_\pi\ 0.604)$ [10] is shown in Fig. 9 (blue line) as a function of interrogation time $T_\pi$. For realistic interrogation times $T_\pi > 100$ ms it is at least one order of magnitude below the systematic uncertainties achieved by optical clocks at present [1, 3]. For Ramsey spectroscopy, we follow the same procedure an take into account the non-zero initial phase of the second pulse (see Fig. 8 red line). Fig. 9 (red line) shows the resulting fractional frequency shift $\Delta y = \Delta p/(\pi\ \nu[T_{\mathrm{d}} + (2 - 4/\pi)T_{\pi/2}])$ [10] as a function of dark time $T_{\mathrm{d}}$ for a realistic $\pi/2$-pulse duration $T_{\pi/2} = 1$ ms. Therefore, frequency shifts resulting from stepping the fundamental beam's power in the scheme shown in Fig. 6 are below state-of-the-art clock's uncertainties for Rabi and Ramsey spectroscopy.

Optics EXPRESS

## 5. Conclusion

Our analysis of phase noise from a PPLN frequency doubler under steady-state conditions gives a limit on doubler-induced phase noise at frequencies smaller than 10 Hz, which is at least 13 dB lower than that of a previous characterization [23]. It shows that no limitation of laser performance due to differential phase noise of the SHG module is to be expected in the foreseeable future (i.e., until ultrastable lasers reach frequency instability on the order of $10^{-19}$) and an optical path length stabilization on the fundamental wavelength can be employed. Our phase characterization with a femtosecond frequency comb results in significantly higher phase noise, which we attribute to the comb or to rf signal processing associated with the comb. For the next generation of clock interrogation lasers, this may become a limiting factor in stability transfer. Furthermore, we have discussed the influence of laser power-induced phase chirps on clock operation in the case of a simple path length stabilization. Resulting frequency shifts can be constrained to below $10^{-19}$ and thus below today's clock uncertainties.

## Funding

Deutsche Forschungsgemeinschaft (DFG, German Research Foundation) (CRC 1128 project A03, CRC 1227 project B02, EXC-2123/1); European Space Agency (ESA) (4000119716).

## Acknowledgments

We would like to thank Thomas Legero and Sebastian Häfner for providing the phase noise curve of [14].

## References

1. S. M. Brewer, J.-S. Chen, A. M. Hankin, E. R. Clements, C. W. Chou, D. J. Wineland, D. B. Hume, and D. R. Leibrandt, "An $^{27}Al^{+}$ quantum-logic clock with systematic uncertainty below $10^{-18}$," Phys. Rev. Lett. **123**, 033201 (2019).
2. C. Sanner, N. Huntemann, R. Lange, C. Tamm, E. Peik, M. S. Safronova, and S. G. Porsev, "Optical clock comparison test of Lorentz symmetry," Nature **567**, 204–208 (2019).
3. W. F. McGrew, X. Zhang, R. J. Fasano, S. A. Schäffer, K. Beloy, D. Nicolodi, R. C. Brown, N. Hinkley, G. Milan, M. Schioppo, T. H. Yoon, and A. D. Ludlow, "Atomic clock performance beyond the geodetic limit," Nature **564**, 87–90 (2018).
4. S. L. Campbell, R. B. Hutson, G. E. Marti, A. Goban, N. Darkwah Oppong, R. L. McNally, L. Sonderhouse, J. M. Robinson, W. Zhang, B. J. Bloom, and J. Ye, "A Fermi-degenerate three-dimensional optical lattice clock," Science **358**, 90–94 (2017).
5. M. Schioppo, R. C. Brown, W. F. McGrew, N. Hinkley, R. J. Fasano, K. Beloy, T. H. Yoon, G. Milani, D. Nicolodi, J. A. Sherman, N. B. Phillips, C. W. Oates, and A. D. Ludlow, "Ultra-stable optical clock with two cold-atom ensembles," Nat. Photonics **11**, 48–52 (2017).
6. A. Al-Masoudi, S. Dörscher, S. Häfner, U. Sterr, and C. Lisdat, "Noise and instability of an optical lattice clock," Phys. Rev. A **92**, 063814 (2015).
7. T. L. Nicholson, S. L. Campbell, R. B. Hutson, G. E. Marti, B. J. Bloom, R. L. McNally, W. Zhang, M. D. Barrett, M. S. Safronova, G. F. Strouse, W. L. Tew, and J. Ye, "Systematic evaluation of an atomic clock at $2 \times 10^{-18}$ total uncertainty," Nat. Com. **6**, 6896 (2015).
8. J. Grotti, S. Koller, S. Vogt, S. Häfner, U. Sterr, C. Lisdat, H. Denker, C. Voigt, L. Timmen, A. Rolland, F. N. Baynes, H. S. Margolis, M. Zampaolo, P. Thoumany, M. Pizzocaro, B. Rauf, F. Bregolin, A. Tampellini, P. Barbieri, M. Zucco, G. A. Costanzo, C. Clivati, F. Levi, and D. Calonico, "Geodesy and metrology with a transportable optical clock," Nat. Phys. **14**, 437–441 (2018).
9. T. Mehlstäubler, G. Grosche, C. Lisdat, P. Schmidt, and H. Denker, "Atomic clocks for geodesy," Rep. Prog. Phys. **81**, 064401 (2018).
10. G. J. Dick, "Local oscillator induced instabilities in trapped ion frequency standards," in *Proceedings of* $19^{th}$ *Annu. Precise Time and Time Interval Meeting, Redendo Beach, 1987,* (U.S. Naval Observatory, Washington, DC, 1988), pp. 133–147.
11. P. G. Westergaard, J. Lodewyck, and P. Lemonde, "Minimizing the Dick effect in an optical lattice clock," IEEE Trans. Ultrason. Ferroelectr. Freq. Control. **57**, 623–628 (2010).
12. W. M. Itano, J. C. Bergquist, J. J. Bollinger, J. M. Gilligan, D. J. Heinzen, F. L. Moore, M. G. Raizen, and D. J. Wineland, "Quantum projection noise: Population fluctuations in two-level systems," Phys. Rev. A **47**, 3554–3570 (1993). See Also: Erratum Phys. Rev. A 51, 1717 (1995).

Optics EXPRESS


13. T. Kessler, T. Legero, and U. Sterr, "Thermal noise in optical cavities revisited," J. Opt. Soc. Am. B **29**, 178–184 (2012).
14. D. G. Matei, T. Legero, S. Häfner, C. Grebing, R. Weyrich, W. Zhang, L. Sonderhouse, J. M. Robinson, J. Ye, F. Riehle, and U. Sterr, "1.5 $\mu$m lasers with sub-10 mHz linewidth," Phys. Rev. Lett. **118**, 263202 (2017).
15. S. Häfner, S. Falke, C. Grebing, S. Vogt, T. Legero, M. Merimaa, C. Lisdat, and U. Sterr, "8 $\times 10^{-17}$ fractional laser frequency instability with a long room-temperature cavity," Opt. Lett. **40**, 2112–2115 (2015).
16. S. Amairi, T. Legero, T. Kessler, U. Sterr, J. B. Wübbena, O. Mandel, and P. O. Schmidt, "Reducing the effect of thermal noise in optical cavities," Appl. Phys. B **113**, 233–242 (2013).
17. G. D. Cole, W. Zhang, M. J. Martin, J. Ye, and M. Aspelmeyer, "Tenfold reduction of Brownian noise in optical interferometry," Nat. Photonics **7**, 644–650 (2013).
18. D. Nicolodi, B. Argence, W. Zhang, R. Le Targat, G. Santarelli, and Y. Le Coq, "Spectral purity transfer between optical wavelengths at the $10^{-18}$ level," Nat. Photonics **8**, 219–223 (2014).
19. C. Hagemann, C. Grebing, T. Kessler, S. Falke, N. Lemke, C. Lisdat, H. Schnatz, F. Riehle, and U. Sterr, "Providing $10^{-16}$ short-term stability of a 1.5 $\mu$m laser to optical clocks," IEEE Trans. Instrum. Meas. **62**, 1556–1562 (2013).
20. S. B. Koller, J. Grotti, S. Vogt, A. Al-Masoudi, S. Dörscher, S. Häfner, U. Sterr, and C. Lisdat, "Transportable optical lattice clock with $7 \times 10^{-17}$ uncertainty," Phys. Rev. Lett. **118**, 073601 (2017).
21. R. L. Sutherland, *Handbook of Nonlinear Optics* (Marcel Dekker,, 2003), 2nd ed.
22. D. Yeaton-Massey and R. X. Adhikari, "A new bound on excess frequency noise in second harmonic generation in PPKTP at the $10^{-19}$ level," Opt. Exp. **20**, 21019–21024 (2012).
23. M. Delehaye, J. Millo, P.-Y. Bourgeois, R. B. Lucas Groult, E. Rubiola, E. Bigler, Y. Kersalé, and C. Lacroûte, "Residual phase noise measurement of optical second harmonic generation in PPLN waveguides," IEEE Phot. Tech. Lett. **29**, 1639–1642 (2017).
24. J. Stenger, H. Schnatz, C. Tamm, and H. R. Telle, "Ultra-precise measurement of optical frequency ratios," Phys. Rev. Lett. **88**, 073601–1–4 (2002).
25. A. D. Ludlow, M. M. Boyd, J. Ye, E. Peik, and P. O. Schmidt, "Optical atomic clocks," Rev. Mod. Phys. **87**, 637–701 (2015).
26. S. Falke, M. Misera, U. Sterr, and C. Lisdat, "Delivering pulsed and phase stable light to atoms of an optical clock," Appl. Phys. B **107**, 301–311 (2012).
27. R. C. Hilborn, "Einstein coefficients, cross sections, f values, dipole moments, and all that," arXiv:physics/0202029 [physics.atom-ph] (2002). This is a revised (February, 2002) version of a paper that originally appeared in Am. J. Phys. 50, 982-986 (1982).
28. M. M. Boyd, T. Zelevinsky, A. D. Ludlow, S. Blatt, T. Zanon-Willette, S. M. Foreman, and J. Ye, "Nuclear spin effects in optical lattice clocks," Phys. Rev. A **76**, 022510–1–14 (2007).